



# Non-Enzymatic Sensing of D-Sorbitol using Polyaniline-Coated Stainless Steel Electrodes

Subrata Mondal, Piyali Bhanja and M.V. Sangaranarayanan\*

**Abstract** | The Potentiodynamic deposition of polyaniline on stainless steel electrodes has been carried out using the anionic surfactant sodium tetradecyl sulphate in the presence of acetic acid. The PANI-coated SS electrode was characterized using different spectroscopic and microscopic techniques. The efficacy of the electrode was analyzed for non-enzymatic sensing of D-sorbitol. Amperometric and impedimetric studies reveal the suitability of the electrode for sensing. A detection limit of 5  $\mu\text{M}$  along with a linear range spanning of 75–637  $\mu\text{M}$  and sensitivity of 0.027  $\mu\text{A } \mu\text{M}^{-1}$  is deduced from the amperometric analysis.

**Keywords:** Polyaniline, D-Sorbitol, Amperometry, Impedimetry

## 1 Introduction

The field of conducting polymers has witnessed rapid strides during the past few decades on account of its diverse applications in energy storage devices,<sup>1–2</sup> biosensors,<sup>3–6</sup> electrocatalysts,<sup>7–9</sup> etc. The chemical synthesis of polypyrrole (PPy), polyaniline (PANI) among various conducting polymers, polyaniline has been widely studied on account of its high conductivity, thermal stability and facile synthetic protocols. These properties in turn lead to impressive applications ranging from biosensors to supercapacitors, polythiophene (PT) and polyindole (PIn) is often accomplished using oxidizing agents. Alternately, these can also be prepared using diverse electrochemical techniques on different substrates.<sup>10–15</sup> The electrochemical techniques are more preferable in view of their tunable thickness *vis a vis* mass loading of polymers. Among various conducting polymers, polyaniline has extensively been employed due to its environmental stability, high conductivity and impressive redox properties. Due to the combination of polymeric properties as well as metallic conductivity, PANI possesses wide range of applications. The chemical and electrochemical synthesis of polyaniline has been carried out using acids such as HCl, H<sub>2</sub>SO<sub>4</sub>, HNO<sub>3</sub>, HClO<sub>4</sub>, *para*-toluene sulphonic acid (P-TSA).<sup>16–20</sup> In recent studies, more emphasis has been placed on synthesis of PANI using surfactants and templates which yield diverse morphologies,

*viz.*, nanofibres,<sup>21–22</sup> nanorods,<sup>23–25</sup> nanospheres,<sup>26</sup> nanotubes,<sup>27</sup> nanosheets,<sup>28</sup> etc.

The occurrence of high sugar in blood arises from diabetics mellitus (DM) and is caused by **D-sorbitol** while the accumulation of D-sorbitol results in laxative effects. Besides, D-sorbitol has a few beneficial effects, e.g., in cosmetic industry for preventing moisture and also in dairy products. Hence it is essential to estimate the amount of D-sorbitol using simple procedures. Several methods have been reported for estimating D-sorbitol, *viz.*, enzymatic techniques,<sup>29</sup> chromatographic methods,<sup>30</sup> etc. These methods have two main limitations, *viz.*, (i) the enzymatic methods employ D-sorbitol dehydrogenase as an enzyme or NAD<sup>+</sup> (Nicotinamide Adenine Dinucleotide) as a coenzyme. The presence of D-sorbitol dehydrogenase interferes with other sugars during the detection of D-sorbitol.<sup>31</sup> On the other hand, when the coenzyme NAD<sup>+</sup> is employed, large applied potentials are required, thereby compromising on the selectivity due to interference from the other electroactive species,<sup>32</sup> and (ii) The chromatographic method is more involved requiring sophisticated protocols. Hence it is essential to develop simple and facile strategies for non-enzymatic detection of D-sorbitol.

Here, we report the electrochemical deposition of polyaniline on a stainless steel substrate employing acetic acid and sodium tetradecyl sulphate (STS). Although acetic acid is a weak electrolyte and

**D-sorbitol:** D-sorbitol is a naturally-occurring polyhydric alcohol and is an isomer of mannitol. It is often employed as a sweetening agent and causes diabetes mellitus if present in large quantities.

Department of Chemistry,  
Indian Institute of  
Technology, Madras-  
Chennai, 600036, India.

\*sangara@iitm.ac.in

is unsuitable for polymerization in general, the presence of STS induces the polymerization of aniline. The use of weak acids in the synthesis of conducting polymers is desirable since the surface is rendered stable under diverse conditions. Among various electrochemical techniques employed here, **amperometry** is capable of yielding satisfactory linear calibration range and low detection limits.

## 2 Experimental

The experimental procedure involves (i) the potentiodynamic polymerization of aniline on stainless steel electrodes, and (ii) the subsequent detection of D-sorbitol using amperometry, differential pulse voltammetry (DPV) and **impedimetry**.

### 2.1 Chemicals

Aniline obtained from Sigma Aldrich was distilled at 140°C under nitrogen atmosphere at reduced pressure and then stored in the refrigerator. Sodium tetradecyl sulphate (STS) obtained from Sigma Aldrich was used as received. D-sorbitol, sodium nitrate and acetic acid were procured from SRL Chemicals India and employed as received.

### 2.2 Electrochemical measurements

Electrochemical measurements were carried out in a one-compartment cell with three-electrode configuration. The experiments involving cyclic voltammetry, chronoamperometry, differential pulse voltammetry (DPV) and Electrochemical Impedance Spectroscopy (EIS) were performed in CH 660 A Electrochemical work station (CH Instruments, USA). All the experiments were carried out at the temperature of  $30 \pm 1^\circ\text{C}$ . A Stainless Steel (SS) substrate of surface area  $1\text{ cm}^2$  is the working electrode for the deposition of PANI while the saturated calomel electrode (SCE) and Pt wire (Bioanalytical systems, USA) serve as the reference and counter electrodes, respectively. The composition of SS electrodes is as follows: 17% chromium, 2.5% nickel and 0.15% carbon. The SS electrode is dipped into concentrated  $\text{H}_2\text{SO}_4$  and then sonicated for ten minutes in triply distilled water. The polymerization of aniline (0.025 M) is carried out potentiodynamically in the potential window from  $-0.7\text{ V}$  to  $+1.2\text{ V}$  for forty cycles under de-aerated conditions using 0.0125 M STS, with and without 0.02 M acetic acid (AA). While the potentiodynamic synthesis of PANI is well-known, the number of cycles and concentration of STS and AA have been optimized here (*vide infra*). After polymerization, the electrodes were washed repeatedly with distilled water and dried. The PANI-coated SS electrode serves as the working electrode

for the electrochemical detection of D-sorbitol. For sensing of D-sorbitol, amperometry, DPV and EIS were employed using 0.2M  $\text{NaNO}_3$ . Before the construction of the calibration curves, the chronoamperometric current response is analyzed to obtain the time required for the steady state. DPV has been carried out for the preliminary investigation regarding sensing aspects with the following parameters: potential increment = 4 mV, amplitude = 50 mV, pulse width = 0.05 sec and pulse period = 0.5 s. The impedance studies were carried out in the frequency range  $10^{-2}$  to  $10^5$  Hz with the amplitude of 5 mV.

### 2.3 Instrumentation

To obtain the FT Raman data, the samples were dissolved in acetone and the spectra were recorded using the Bruker RFS 27: stand-alone spectrometer with the laser source of Nd: YAG 1064 nm (resolution being  $2\text{ cm}^{-1}$ ).

The UV-Visible absorption spectra were obtained using Jasco V-650 spectrophotometer and Ocean Optics GmbH DT-MINI-2-GS UV-Vis spectrophotometer. The SEM images were acquired using FEI Quanta FEG 200 at an acceleration voltage of 10–20 kV in high vacuum mode. The X-ray diffraction (XRD) analysis was carried out by Bruker D<sub>8</sub> Advance equipped with Cu K $\alpha$  radiation ( $1.5405\text{ \AA}$ ).

## 3 Results and Discussion

### 3.1 Cyclic voltammograms of PANI

Figure 1 depicts the cyclic voltammograms pertaining to the deposition of PANI on the SS electrode. The anodic peak at 0.25V is due to the oxidation of PANI as well as doping of the STS anions, i.e.,  $[\text{CH}_3(\text{CH}_2)_{13}\text{OSO}_3]^-$ , while the cathodic peak at  $-0.5\text{ V}$  denotes the reduction of PANI as well as de-doping of STS anions. As the polymerization proceeds, both the oxidation and reduction peak potentials shift towards more positive and negative values, respectively. The thickness of the polymer film increases with the number of cycles; however, the number of cycles needs to be optimized depending on the application required. In the case of Fig. 1(B), there are no prominent redox peaks during polymerization, thus indicating the less redox active feature of PANI. However, the magnitude of current in Fig. 1(B) is larger than in Fig. 1(A) since the concentration of the surfactant (0.1 M) chosen is higher than 0.0125 M so as to decipher whether STS alone is adequate for the deposition of PANI. The mechanism of polymerization is as follows. Aniline monomers yield the radical cations via

**Amperometry:** Amperometry is a facile analytical technique which provides the systematic variation of the current with sequential additions of the analytes. It is a powerful technique in view of its wide linear calibration range and high sensitivity.

**Impedimetry:** A suitable system parameter (e.g. charge transfer resistance) is analysed at an optimum potential over a wide frequency ranges. A calibration curve is drawn using the charge transfer resistances as a function of the analyte concentrations.

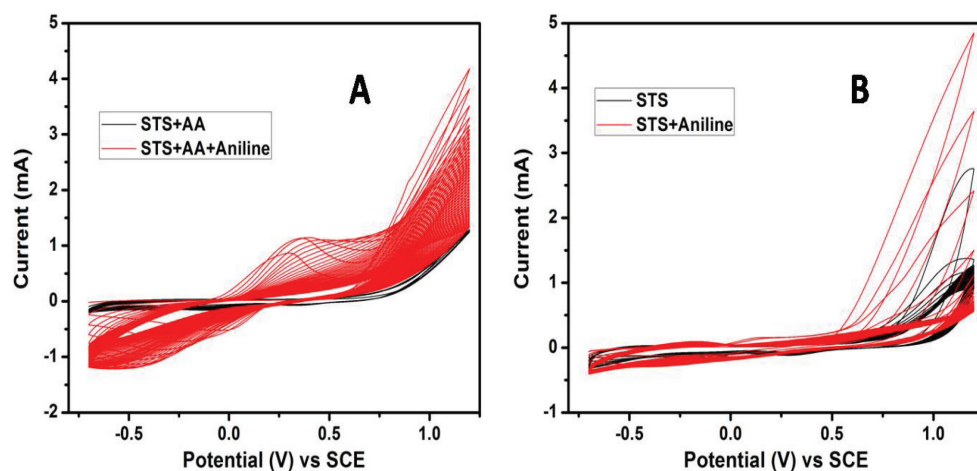


**Figure 1:** Cyclic voltammogram depicting the polymerization of aniline on SS electrodes at a scan rate of 0.1 V/s using (A) 0.0125 M STS + 0.02 M AA and (B) 0.1 M STS alone. Number of cycles = 40. The voltammetric response of the SS electrode in the blank solution (without aniline) is also shown.

oxidation and subsequently the combination of two monomer radical cations occurs, followed by the removal of two  $H^+$  ions. The re-oxidation, coupling and de-protonation processes continue during the propagation step so as to yield PANI.

It is essential here to analyze the influence of the concentration of STS as regards the formation of PANI on the electrode. Although increasing the concentration of STS enhances the current response, large concentrations of STS in the presence of AA leads to a precipitate. On the other hand, at low surfactant concentrations, the extent of polymerization is lower. Hence the optimized concentration of STS is chosen here. Indeed, a larger concentration of surfactant is chosen here during the deposition of PANI, since it functions both as a supporting electrolyte and surfactant. The thickness ( $d$ ) of the PANI film is estimated from the formula  $d = QM_w / ZFA\rho$  using the charge ( $Q$ ) passed during the polymerization reaction, where  $M_w$  denotes the molecular weight of aniline ( $M_w = 93.1$  g/mol),  $\rho$  being its density ( $\rho = 1.02$  g/ml),  $A$  denotes the geometrical area of the electrode ( $1$  cm<sup>2</sup>) and  $z$  represents the number of electrons per aniline unit ( $z = 0.5$ ). The estimated thickness of PANI film is the  $\sim 2$   $\mu$ m.

### 3.2 Characterization of PANI-coated SS electrodes

The PANI-coated SS electrode was subjected to FT-Raman, UV-visible spectroscopy as well as SEM studies.

**3.2.1 FT-Raman spectroscopy:** The FT-Raman spectroscopy is complementary to FT-IR analysis and provides information on various vibrational

modes. The FT-Raman spectra are shown in Fig. 2. The band observed at  $1600$  cm<sup>-1</sup> is due to C=C stretching while the weak band at  $1508$  cm<sup>-1</sup> arises from the C=N stretching vibration. The intense band at  $1352$  cm<sup>-1</sup> represents the C-N<sup>+</sup> stretching vibration of semiquinoid ring of PANI. Further, the band noticed at  $ca$   $1180$  cm<sup>-1</sup> is due to the in-plane bending of C-H for both quinoid and benzenoid ring of polymer. These Raman spectral data are consistent with the previously reported values regarding the position of the bands.<sup>33</sup> There are no significant differences between the two PANI samples (with and without STS). Although the peak positions are similar for both the samples, the peak intensities are dissimilar. The higher peak intensities for PANI prepared in the presence of STS and AA signify the larger extent of deposition than that of STS alone.

**3.2.2 UV-Visible spectra:** Figure 2(B) depicts the UV-Vis spectra of PANI synthesized using (a) STS+AA and (b) STS. An intense peak at  $331.1$  nm is observed along with weak and broad absorption bands at  $407.4$  and  $409.8$  nm for both the PANI samples prepared using STS in the (a) presence and (b) absence of AA, respectively. The peak at  $331.1$  nm is due to the  $\pi \rightarrow \pi^*$  transition while that at  $400$  nm is attributed to  $n \rightarrow \pi^*$  transition. The broad bands near  $550$  and  $700$  nm correspond to the polaron-bipolaron transition and benzenoid-quinoid excitation transitions.<sup>34</sup>

**3.2.3 Scanning Electron Microscopic studies:** Figure 2(C) depicts the SEM images wherefrom uniform and non-aggregated distribution of nanospheres with diameters of  $50$ – $100$  nm is

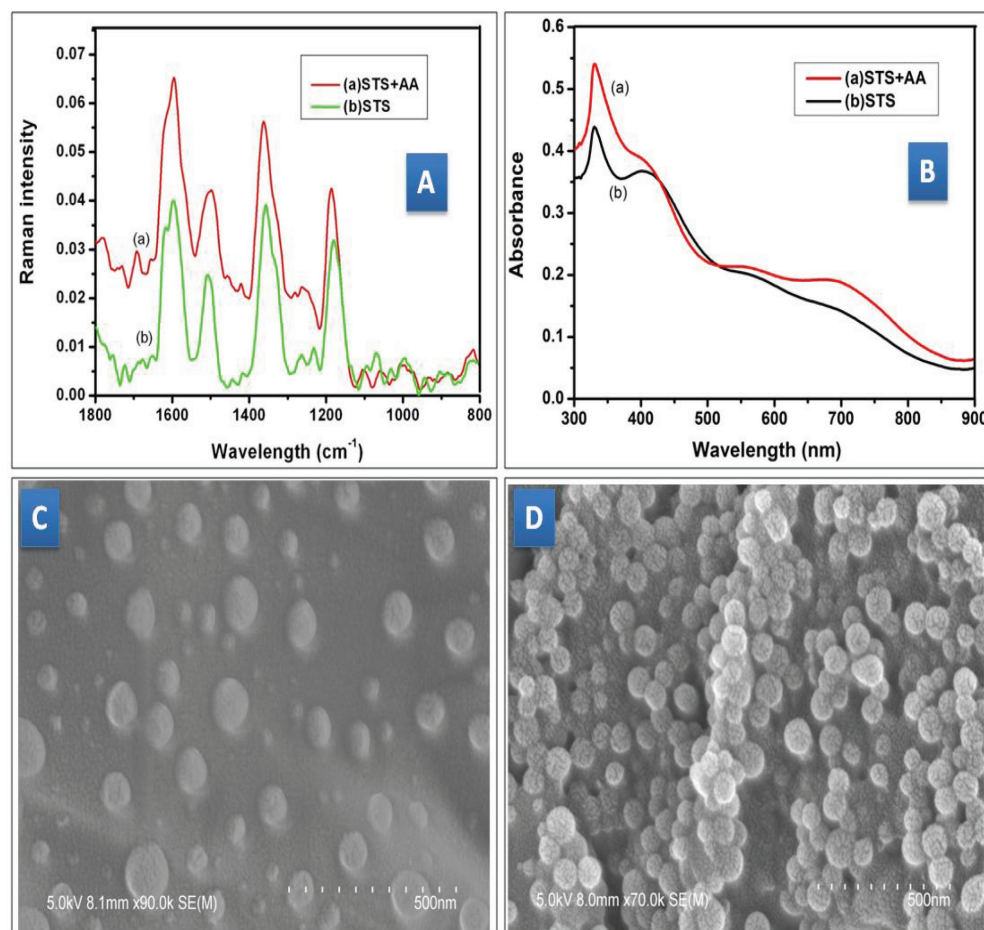


**Figure 2:** (A) FT-Raman and (B) UV-Vis spectra of PANI prepared using (a) STS + AA, and (b) STS alone. Typical SEM images of PANI prepared in the presence of (C) STS + AA and (D) STS alone.

inferred for the PANI synthesized in the presence of AA and STS on SS electrode (Fig. 2C). However, the sizes of these spheres are not uniform. In the case of PANI synthesized using STS alone, aggregated nanospheres with the diameter of 50–80 nm are noticed and the particles are smaller as shown in Fig. 2D. The mechanism behind the formation of PANI nanospheres can be postulated in the following manner: In the presence of STS, the aniline monomers diffuse to the spherical micelles of the surfactant (here STS) and the polymerization occurs into the micelles deposited on the SS electrode, thereby yielding spherical geometries. At low surfactant concentrations, the PANI nanospheres are well separated and non-aggregated while the aggregation occurs at higher concentrations.

**3.2.4 XRD studies:** Figure 3 depicts the XRD patterns of the SS electrodes and the reflections at  $2\theta$  values of  $45^\circ$ ,  $52^\circ$  and  $75^\circ$  correspond to the SS. The XRD pattern of PANI exhibits a

broad band at diffraction angle of  $28.15^\circ$  and  $27.38^\circ$ , which indicates the amorphous nature of polyaniline obtained with and without STS. The d-spacing between the crystal planes was calculated from the Bragg equation  $n\lambda = 2d\sin\theta$ , where  $n$  is an integer,  $\lambda$  is the wavelength of the CuK $\alpha$  radiation source ( $\lambda = 1.5406 \text{ \AA}$ ) and  $\theta$  is the angle between incident radiation and crystal planes. For PANI, the characteristic is peak observed at  $2\theta$  values of  $28.15^\circ$  and  $27.38^\circ$ , and the calculated d-spacing values are 3.169 and 3.264  $\text{\AA}$ , respectively. Furthermore, the  $2\theta$  value for PANI prepared in the absence of AA is larger.

### 3.3 Detection of D-sorbitol using the PANI-coated SS electrode

From the forgoing study, it is seen that although PANI is formed on the SS electrodes even with STS alone, the effective polymerization occurs in the presence of STS and AA. In view of this, the PANI coated on SS electrode in the presence of

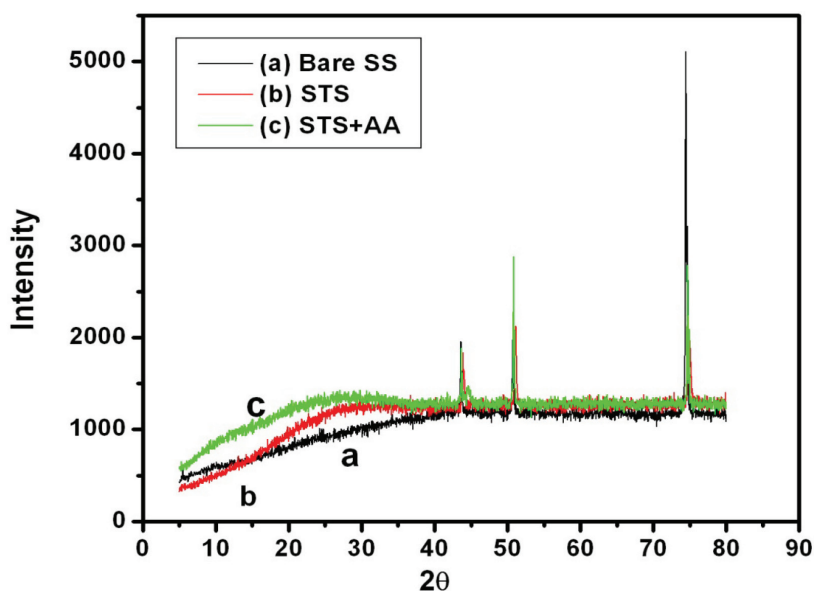


**Figure 3:** The XRD pattern of (a) bare SS and PANI-coated SS electrode in the presence of (b) STS, and (c) STS + AA.

STS+AA is employed as the working electrode and is designated as PANI/SS.

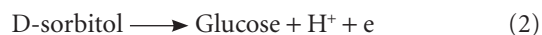
**3.3.1 Differential Pulse Voltammetry:** It is customary to employ DPV in electroanalytical chemistry since it has the ability to detect nanomolar concentrations with common planar working electrodes. Hence we carried out the preliminary studies using DPV (Fig. 4). At different concentrations of the analyte, the shift in peak potentials occurred instead of the systematic variation in the peak current, thus precluding the detection of D-sorbitol using DPV. While this shift in the peak potentials rather than the increase in the peak current requires further studies, a plausible origin of this behaviour may lie in the hindrance of electron transfer between PANI and D-sorbitol.

A plausible mechanism for the sensing of D-sorbitol can be postulated as follows:

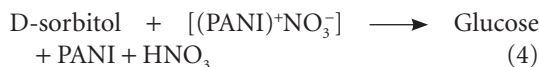
The oxidation of PANI in  $\text{NaNO}_3$  before the addition of D-sorbitol is as follows:



After adding D-sorbitol the oxidation may be represented as,



Thus, the overall reaction is given by,



**3.3.2 Amperometric detection:** In amperometric sensing, a suitable potential is applied as an input and the steady-state current is measured at various analyte (D-sorbitol) concentrations. The PANI/SS electrode is initially dipped in 0.2 M  $\text{NaNO}_3$  so as to estimate the current for the blank solution. Subsequently, 25  $\mu\text{L}$  of 0.01 M D-sorbitol is added successively and the current is noticed. In order to ensure complete mixing and to reach the steady state, a time interval of 40 s is allowed before each addition of D-sorbitol. Figure 5 depicts the amperometric response of the PANI/SS electrode wherein the decrease in the amperometric current with the successive additions of D-sorbitol is observed for both the potentials. The stepwise decrease in current after each addition is indicative of the linear response of the PANI/SS electrode for the sensing of D-sorbitol. The typical  $i-t$  response pertaining to the diffusion-controlled process enables the construction of the calibration curve shown in Fig. 5. Furthermore, it can be inferred from Fig. 4 that the PANI/SS electrode exhibits a higher sensitivity and lower limit of detection at 0.5 V than at 0.2 V.

To further improve the linear range of the PANI/SS electrode, amperometric studies were carried out with successive addition of 25  $\mu\text{L}$  of 0.015 M solution of D-sorbitol, after fixing the potential as 0.5 V. The PANI/SS electrode

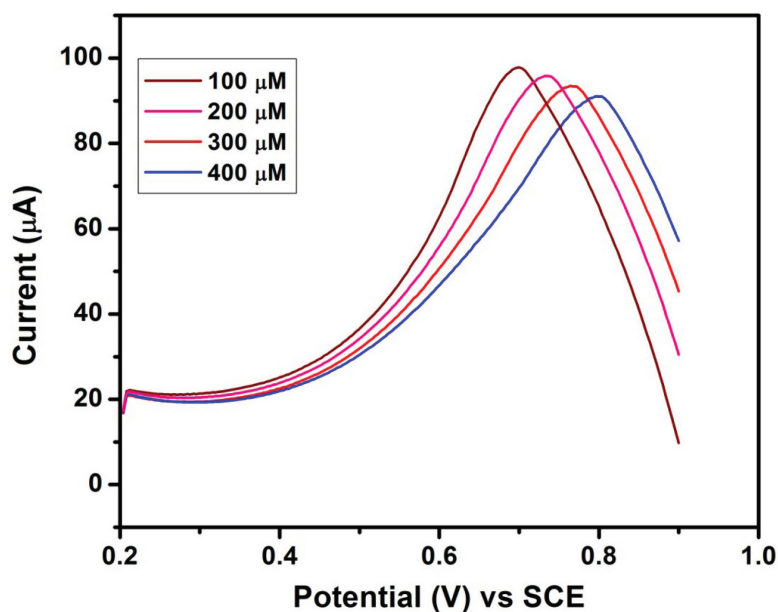
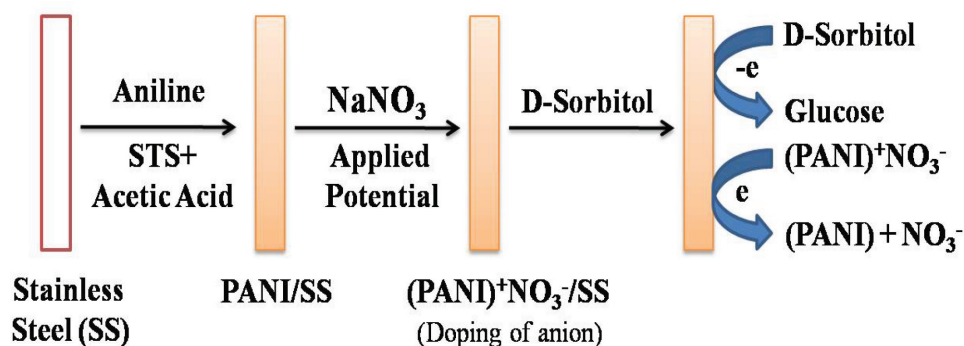


**Figure 4:** Differential Pulse Voltammogram of the PANI/SS electrode in 0.2 M  $\text{NaNO}_3$  solution for various concentrations of D-sorbitol.



**Scheme 1:** A schematic representation of the sensing of D-sorbitol using the PANI/SS electrode.

exhibits a systematic decrease in current with the successive additions of D-sorbitol (Fig. 6). The sensitivity refers to the change in current response per unit concentration of the analyte per unit area of the electrode and a sensitivity of  $0.027 \mu\text{A } \mu\text{M}^{-1}$  is deduced with the linear range spanning  $75 \mu\text{M}$  to  $637 \mu\text{M}$  concentrations of D-sorbitol. As the linearity is invalid beyond  $637 \mu\text{M}$  concentration of D-sorbitol it may be attributed to the alteration in the redox properties of PANI. The limit of detection (LOD) is estimated as  $5 \mu\text{M}$  from the equation  $\text{LOD} = 3\sigma/l$ , where  $\sigma$  is the standard deviation obtained from the blank current (current in the absence of Sorbitol) and  $l$  is the slope of the calibration plot of Sorbitol (inset of Fig. 6). The response time defined as the time

required to sense 90% change in the D-sorbitol concentration ( $t_{90}$ ) is  $\sim 5$  s.

### 3.3.3 Electrochemical Impedance Spectroscopy:

Electrochemical Impedance Spectroscopy (EIS) is a valuable technique for obtaining various system parameters of electrochemical systems. The impedance data can be represented using Bode' magnitude, Bode' phase angle and Nyquist plots.<sup>35</sup> The Nyquist plot which depicts the real and imaginary parts of the impedance at different frequencies is a convenient method for constructing the calibration curve for sensing analytes. Figure 7(A) depicts the Nyquist plots pertaining to the PANI/SS electrode for various concentrations of D-sorbitol at 0.2V

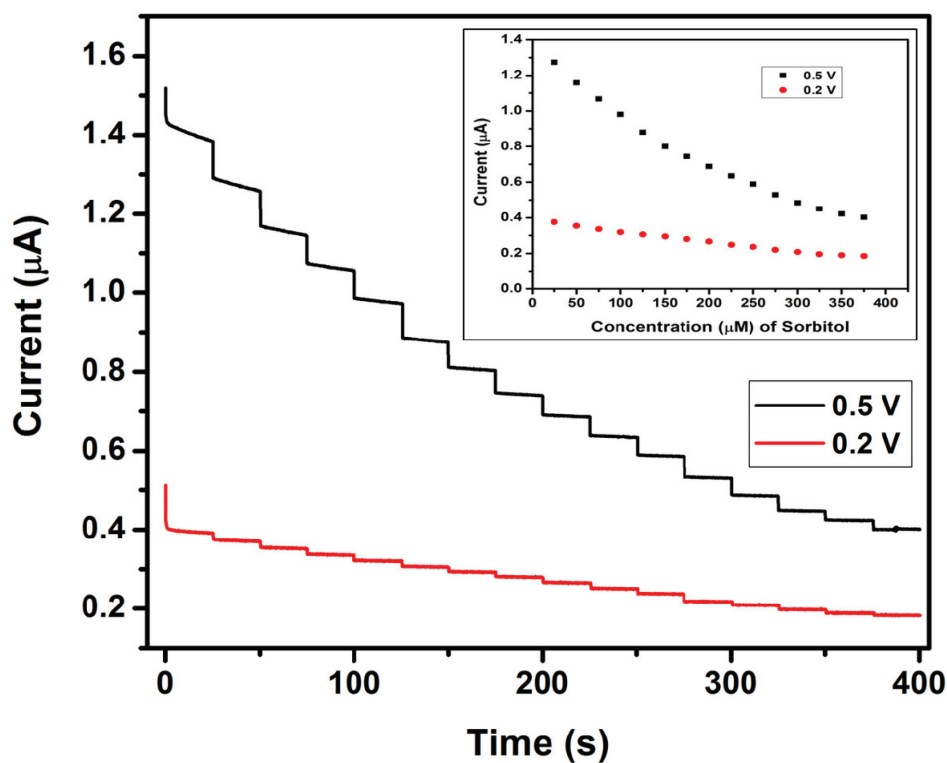


**Figure 5:** Chronoamperometric current response of the PANI/SS electrode in 0.2 M NaNO<sub>3</sub> solution for successive additions of 25 μL of 0.01 M D-sorbitol at two potentials. The inset depicts the variation in the steady-state current with concentration.

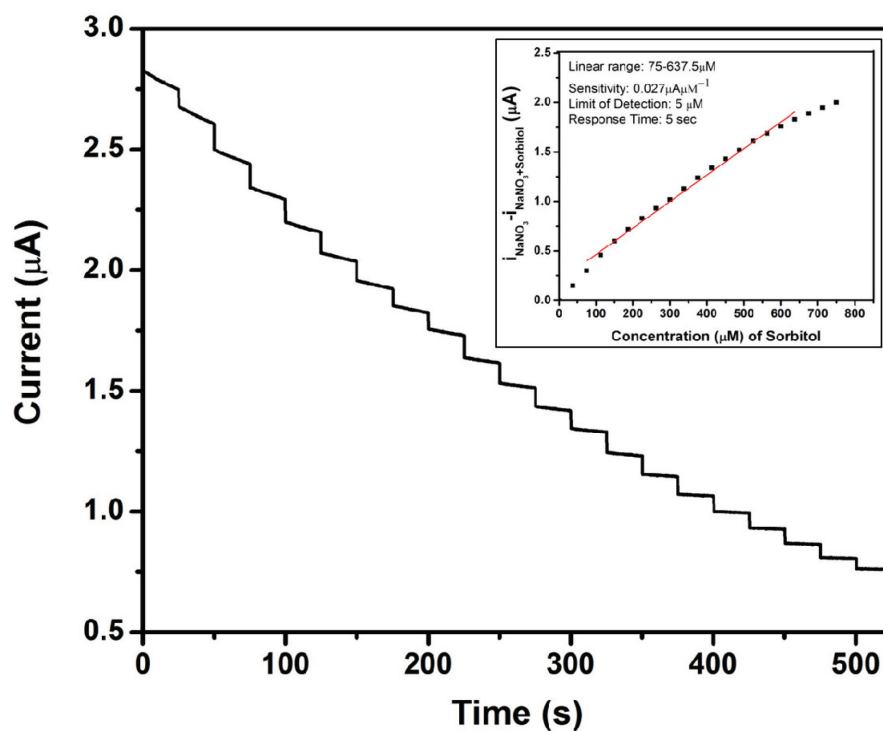


**Figure 6:** Chronoamperometric current response of the PANI/SS electrode in 0.2 M NaNO<sub>3</sub> solution with the successive additions of 25 μL of 0.015 M D-sorbitol solution at a constant potential of 0.5 V. The inset depicts the calibration curve drawn after taking into account the current for the blank solution.

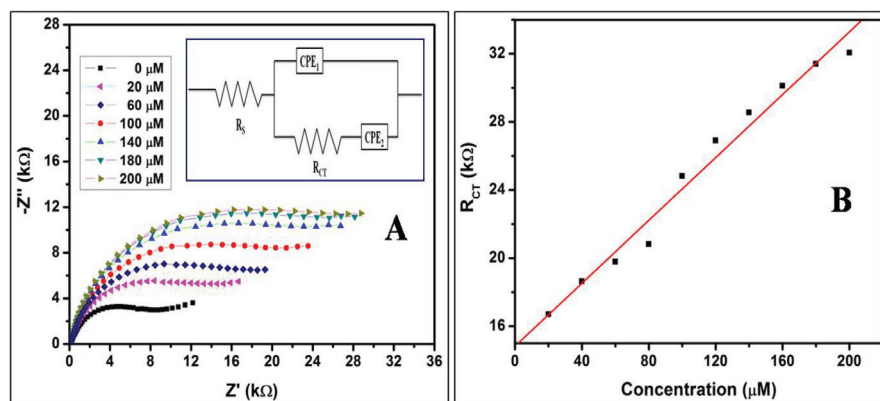


**Figure 7:** (A) Nyquist plots of the PANI/SS electrode in 0.2 M NaNO<sub>3</sub> solution at 0.2 V for various concentrations of D-sorbitol and (B) The calibration curve is drawn using the charge transfer resistances. The inset in A represents the equivalent circuit employed for fitting the Nyquist plots.

**Table 1:** System parameters obtained from the fitting of the Nyquist plots to the equivalent circuit shown in Fig. 7.

Concentration of Sorbitol	$R_s$ ( $\Omega$ )	$R_{CT}$ ( $k\Omega$ )	$CPE_1$ (in $10^{-5} \Omega s^{-1}$ )	$n_1$	$CPE_2$ (in $10^{-3} \Omega s^{-1}$ )	$n_2$
40 $\mu$ M	25	18.63	5.5	0.77	1.2	0.69
100 $\mu$ M	25	24.89	5.5	0.78	1.0	0.69
140 $\mu$ M	25	28.55	5.5	0.78	1.1	0.69
180 $\mu$ M	25	30.12	5.5	0.79	1.0	0.69
200 $\mu$ M	25	32.06	5.5	0.79	1.1	0.69

(The circuit parameters given above have a mean absolute error of 2%).

wherein pseudo-semi circles are noticed at high frequencies. When the potential is made more positive or negative (than 0.2V), the Nyquist plots did not exhibit significant variation for different concentrations. Hence the optimum potential for impedance analysis was chosen as 0.2 V. The intercept of the semicircle at high frequencies yields the ohmic resistance ( $R_s$ ), while the diameter of the semi-circle provides the charge transfer resistance ( $R_{CT}$ ) of the system.

The equivalent circuit employed for fitting the Nyquist plots is shown in the inset of Fig. 7(A). The classical Randles circuit has been modified here by employing two constant phase elements ( $CPE_1$  and  $CPE_2$ ), without the Warburg component. Table 1 provides the system parameters obtained from the fitting of the Nyquist plots at different concentrations of D-sorbitol.

The calibration curve drawn using the variation of  $R_{CT}$  with the concentration of D-sorbitol is depicted in Fig. 7(B). The observed increase in  $R_{CT}$  with the concentration can be interpreted by invoking the definition of  $R_{CT}$  as  $R_{CT} = RT/nF_i_0$ , where  $i_0$  denotes the exchange current density. The exchange current density ( $i_0$ ) is a measure

of the rate of electron transfer between PANI film and D-sorbitol and since  $R_{CT}$  increases with concentration,  $i_0$  decreases correspondingly. Due to the absorption of the analyte on the PANI films, the electron transfer rate constant *vis a vis* current decreases with the concentration. This current response behaviour is consistent with the amperometric data. Although  $R_{CT}$  increases with the concentration of D-sorbitol (Fig. 7B), the linear range is noticed only between 20 to 200  $\mu$ M in contrast to the calibration curve from the amperometric data. The sensing characteristics of the present PANI/SS electrode towards D-sorbitol are compared with a few other typical studies in Table 2.

### 3.4 Perspectives and Summary

Although acetic acid (AA) in itself is not suitable for polymerization of aniline on account of its weak dissociation, the addition of the surfactant (STS) induces the deposition of PANI on the electrode surface. In the presence of STS, due to the facile protonation, the dissociation of AA occurs during the polymerization of aniline via radical mechanism. Furthermore, electropolymerization

**Table 2:** An overview of sensors for D-sorbitol.

System	Lowest detection limit	Response time (sec)	Linear range	Ref.
PPD/SDH-NADC/CPE	40 $\mu$ M	40 s	20–800 $\mu$ M	[29]
GCE/MWCNT-PMG/TEOS-PEI-SDH-NADGPS	0.1 mM	—	0.1–4.5 mM	[36]
Au electrode (HPAEC-PAD)	0.03 ng	—	0.01–50 $\mu$ g/g	[30]
PANI/SS	5 $\mu$ M	5 s	75–637 $\mu$ M	This Work

PPD: poly(*o*-phenylenediamine); SDH: D-sorbitol dehydrogenase; NADC: nicotinamide adenine dinucleotide; CPE: carbon paste electrode; GCE: Glassy carbon electrode; MWCNT: Multiwalled carbon nanotubes; PMG: poly(methylene) green; TEOS: Tetraethoxysilane; PEI: poly(ethyleneimine); NADGPS: HPAEC: high-performance anion exchange chromatography; PAD: Pulsed amperometric detector.

using STS and AA is found to be more effective than STS alone, presumably due to the enhanced proton source. While electrochemical polymerization of PANI on various substrates yields nanograins,<sup>37</sup> nanowires,<sup>38–39</sup> etc., the occurrence of nanospheres with dimensions of ~100 nm using a simple synthetic protocol is observed here.

It is of interest to mention here the typical applications of conducting polymer-coated SS substrates as supercapacitors<sup>40</sup> and corrosion inhibitors.<sup>41</sup> Indeed, the conducting polymer-modified SS electrodes have not been extensively studied as sensors. However, we have demonstrated here, the non-enzymatic sensing of D-sorbitol using PANI/SS electrodes. Among the various enzymatic sensing protocols for D-sorbitol, the methodology based on NAD-dependent d-sorbitol dehydrogenase (DSDH) immobilized in a sol–gel carbon nanotube–poly(methylene green) composite deserves mention.<sup>42</sup> The optimization of sensing parameters as well as the influence of other interfering agents in the sensing of D-sorbitol needs to be studied.

In summary, we have carried out the potentiodynamic polymerization of aniline on stainless steel electrodes using acetic acid in the presence of sodium tetradecylsulphate. While the use of strong acids for electrochemical polymerization is well known, the efficacy of acetic acid in conjunction with inexpensive stainless steel electrodes is demonstrated here. Although the differential pulse voltammetric and impedance analysis too can lead to sensing of D-sorbitol, the amperometric measurements provide a satisfactory linear range and low detection limit.

### Acknowledgements

SM thanks the CSIR for the award of Senior Research Fellowship. The helpful comments of the reviewers are gratefully acknowledged. We thank the DST for financial support.

Received 12 August 2016.

### References

- Z. Wang, D.O. Carlsson, P. Tammela, K. Hua, P. Zhang, L. Nyholm, and M. Stromme, Surface Modified Nanocellulose Fibers Yield Conducting Polymer-Based Flexible Supercapacitors with Enhanced Capacitances, *ACS Nano*, **9**, 7563–7571 (2015).
- A. Chandrasoma, R. Grant, A.E. Bruce, M.R.M. Bruce, Electrochemical polymerization of aniline on carbon–aluminum electrodes for energy storage, *J. Power Sources*, **219**, 285–291 (2012).
- Q. Sheng, M. Wang, J. Zheng, A novel hydrogen peroxide biosensor based on enzymatically induced deposition of polyaniline on the functionalized graphene–carbon nanotube hybrid materials, *Sens. Actuators B*, **160**, 1070–1077 (2011).
- S. Singh, P.R. Solanki, M.K. Pandey, B.D. Malhotra, Cholesterol biosensor based on cholesterol esterase, cholesterol oxidase and peroxidase immobilized onto conducting polyaniline films, *Sens. Actuators B*, **115**, 534–541 (2006).
- N.G.R. Mathebe, A. Morrin, E.I. Iwuoha, Electrochemistry and scanning electron microscopy of polyaniline/peroxidase-based biosensor, *Talanta*, **64**, 115–120 (2004).
- H. Zhou, H. Chen, S. Luo, J. Chen, W. Wei, Y. Kuang, Glucose biosensor based on platinum microparticles dispersed in nano-fibrous polyaniline, *Biosens. Bioelectron.*, **20**, 1305–1311 (2005).
- Y. Wang, B. Li, L. Zeng, D. Cui, X. Xiang, W. Li, Polyaniline/mesoporous tungsten trioxide composite as anode electrocatalyst for high-performance microbial fuel cells, *Biosens. Bioelectron.*, **41**, 582–588 (2013).
- Y.F. Huang, C.W. Lin, C.S. Chang, M.J. Ho, Alternative platinum electrocatalyst supporter with micro/nanostructured polyaniline for direct methanol fuel cell applications, *Electrochim. Acta*, **56**, 5679–5685 (2011).
- S. Liu, H. Xu, J. Ou, Z. Li, S. Yang, J. Wang, A feasible approach to the fabrication of gold/polyaniline nanofiber composites and its application as electrocatalyst for oxygen reduction, *Mat. Chem. Phys.*, **132**, 500–504 (2012).

10. J. Molina, A.I. del Río, J. Bonastre, F. Cases, Electrochemical polymerisation of aniline on conducting textiles of polyester covered with polypyrrole/AQSA, *Eur. Polym. J.*, **45**, 1302–1315 (2009).
11. L.T. Qu, L.C. Li, V. Bajpai, G.Q. Shi, L. Dai, Conducting polymer and carbon mesoporous structures by electrochemical syntheses, *Stud. Surf. Sci. Catal.*, **156**, 505–516 (2005).
12. J. Molina, J. Fernández, A.I. del Río, J. Bonastre, F. Cases, Electrochemical synthesis of polyaniline on conducting fabrics of polyester covered with polypyrrole/PW<sub>12</sub>O<sub>40</sub><sup>3-</sup>. Chemical and electrochemical characterization, *Synth. Met.*, **161**, 953–963 (2011).
13. S. Awasthi, A. Srivastava, M.L. Singla, Electrochemical synthesis of novel conducting polymer composite: Polypyrrole–pentacyanonitrosylferrate, *Synth. Met.*, **160**, 1401–1404 (2010).
14. J.M. Freitas, M.L. Duarte, T. Darbre, L.M. Abrantes, Electrochemical synthesis of a novel conducting polymer: The poly[(3-pyrrolyl)-octanoic acid], *Synth. Met.*, **155**, 549–554 (2005).
15. K.M. Ziadan, K.A. Haykaz, A.Q. Abudalla, Some electrical properties of soluble conducting polymer polyhexylthiophene (PHT) prepared by electrochemical polymerization, *Energy Procedia*, **18**, 1059–1067 (2012).
16. M. Delvaux, J. Duchet, P.Y. Stavaux, R. Legras, S.D. Champagne, Chemical and electrochemical synthesis of polyaniline micro- and nano-tubules, *Synth. Met.*, **113**, 275–208 (2000).
17. J.M. Kinyanjui, N.R. Wijeratne, J. Hanks, D.W. Hatchett, Chemical and electrochemical synthesis of polyaniline/platinum composites, *Electrochim. Acta*, **51**, 2825–2835 (2006).
18. N. Plesu, A. Kellenberger, M. Mihali, N. Vaszilcsin, Effect of temperature on the electrochemical synthesis and properties of polyaniline films, *J. Non-Cryst. Solids*, **356**, 1081–1088 (2010).
19. M. Nagaraja, J. Pattar, N. Shashank, J. Manjanna, Y. Kamada, K. Rajanna, H.M. Mahesh, Electrical, structural and magnetic properties of polyaniline/pTSA-TiO<sub>2</sub> nanocomposites, *Synth. Met.*, **159**, 718–722 (2009).
20. R. Pauliukaite, C.M.A. Brett, A.P. Monkman, Polyaniline fibres as electrodes: Electrochemical characterization in acid solutions, *Electrochim. Acta*, **50**, 159–167 (2004).
21. Z. Gao, W. Yang, J. Wang, H. Yan, Y. Yao, J. Ma, B. Wang, M. Zhang, L. Liu, Electrochemical synthesis of layer-by-layer reduced graphene oxide sheets/polyaniline nanofibers composite and its electrochemical performance, *Electrochim. Acta*, **91**, 185–194 (2013).
22. F. Wang, W. Wang, B. Liu, Z. Wang, Z. Zhang, Copolypeptide-doped polyaniline nanofibers for electrochemical detection of ultratrace trinitrotoluene, *Talanta*, **79**, 376–382 (2009).
23. Z. Zhu, G. Wang, M. Sun, X. Li, C. Li, Fabrication and electrochemical characterization of polyaniline nanorods modified with sulfonated carbon nanotubes for supercapacitor applications, *Electrochim. Acta*, **56**, 1366–1372 (2011).
24. H. Peng, G. Ma, W. Ying, A. Wang, H. Huang, Z. Lei, In situ synthesis of polyaniline/sodium carboxymethyl cellulose nanorods for high-performance redox supercapacitors, *J. Power Sources*, **211**, 40–45 (2012).
25. M. Zhang, A. Yamaguchi, K. Morita, N. Teramae, Electrochemical synthesis of Au/polyaniline–poly(4-styrenesulfonate) hybrid nanoarray for sensitive biosensor design, *Electrochem. Commun.*, **10**, 1090–1093 (2008).
26. L. Li, G. Yan, J. Wu, X. Yu, Q. Guo, Preparation of polyaniline–metal composite nanospheres by in situ microemulsion polymerization, *J. Colloid Interface Sci.*, **326**, 72–75 (2008).
27. Z. Wang, Y. Wang, X. Hao, S. Liu, G. Guan, A. Abudula, An all cis-polyaniline nanotube film: Facile synthesis and applications, *Electrochim. Acta*, **99**, 38–45 (2013).
28. H.K. Seo, S. Ameen, M.S. Akhtar, H.S. Shin, Structural, morphological and sensing properties of layered polyaniline nanosheets towards hazardous phenol chemical, *Talanta*, **104**, 219–227 (2013).
29. S.B. Saidman, M.J. Lobo-Castanon, A.J. Miranda-Ordieres, P. Tunon-Blanco, Amperometric detection of d-sorbitol with NAD<sup>+</sup>-d-sorbitol dehydrogenase modified carbon paste electrode, *Analytica Chimica Acta*, **424**, 45–50 (2000).
30. H.J. Sim, J.S. Jeong, H.J. Kwon, T.H. Kang, H.M. Park, Y.M. Lee, S.Y. Kim, S.P. Hong, HPLC with pulsed amperometric detection for sorbitol as a biomarker for diabetic neuropathy, *J. Chromatogr. B*, **877**, 1607–1611 (2009).
31. H.P. Anaja, Diagnostic performance of red cell sorbitol assay in a Nigerian teaching hospital, *Clinica Chimica Acta*, **262**, 1–11 (1997).
32. S. Kwang-Hyok, P. Ui-Nam, C. Sarkar, R. Bhadra, A sensitive assay of red blood cell sorbitol level by high performance liquid chromatography: potential for diagnostic evaluation of diabetes, *Clinica Chimica Acta*, **354**, 41–47 (2005).
33. A.E. Job, C.J.L. Constantino, T.S.G. Mendes, M.Y. Teyura, N. Alves, L.H.C. Mattoso, Effect of natural rubber latex on conducting state of polyaniline blends determined by Raman spectroscopy, *J. Raman Spectrosc.*, **34**, 831–836 (2003).
34. K. Mallick, M. Witcomb, M. Scurrill, A. Strydom, Paramagnetic polyaniline nanospheres, *Chem. Phys. Lett.*, **494**, 232–236 (2010).
35. A.J. Bard, L.R. Faulkner, *Electrochemical Methods: Fundamentals and Applications*, 2nd ed. Wiley, New York (2001).
36. Z. Wang, M. Etienne, S. Pceller, W. Schuhmann, G.-W. Kohring, Victor Mamane, A. Walcarius, Dehydrogenase-based reagentless biosensors: Electrochemically assisted deposition of Sol-Gel thin films on functionalized carbon nanotubes, *Electroanalysis*, **24**, 376–385 (2012).

37. D.S. Dhawale, A. Vinu, C.D. Lokhandea, Stable nanostructured polyaniline electrode for supercapacitor application, *Electrochimica Acta*, **56**, 9482–9487 (2011).
38. V. Gupta, N. Miura, Electrochemically deposited polyaniline nanowire's network. A high-performance electrode material for redox supercapacitor, *Electrochem. Solid-State Lett.*, **8**, A630–A632 (2005).
39. S. Jiao, J. Tu, C. Fan, J. Hou, D.J. Fray, Electrochemically assembling of a porous nano-polyaniline network in a reverse micelle and its application in a supercapacitor, *J. Mat. Chem. A*, **21**, 9027–9030 (2011).
40. T.C. Girija, M.V. Sangaranarayanan, Investigation of polyaniline-coated stainless steel electrodes for electrochemical supercapacitors, *Synth. Met.*, **156**, 244–250 (2006).
41. T., Tuken, B. Yazici, M. Erbil, Zinc modified polyaniline coating for mild steel protection, *Mater. Chem. Phys.*, **99**, 459–464 (2006).
42. Z. Wang, Z., M. Etienne, V. Urbanova, G.-W. Kohring, A. Walcarius *Anal. Bioanal. Chem.*, **405**, 3899–3906 (2013).



**Subrata Mondal** is a senior research fellow at the Department of Chemistry, Indian Institute of Technology Madras under the guidance of Prof. M.V. Sangaranarayanan. His research interests are in the development of novel synthetic methodologies for conducting polymers and their diverse applications.



**Piyali Bhanja** has graduated with B.Sc honours from Jadavpur University and completed her M.Sc in Chemistry from the Indian Institute of Technology, Madras in 2013. Currently, she is pursuing her Ph.D under the guidance of Prof. Asim Bhaumik at the Indian Association for the Cultivation of Science, Kolkata. Her research interests are in the synthesis and applications of metal phosphonates and polymers.



**M.V. Sangaranarayanan** obtained his Ph.D from the Indian Institute of Science, Bangalore and was subsequently an Alexander von Humboldt Fellow with Prof Wolfgang Schmickler. Currently he is a Professor at the Department of Chemistry, Indian Institute of Technology Madras. He has published nearly 120 papers in refereed International journals. His areas of research include statistical mechanics of electrochemical interfaces, diffusion at ultramicroelectrodes, Conducting polymers, sensors, and supercapacitors.

